Journal of Computational and Applied Mathematics 233 (2009) 1139–1154

Contents lists available at ScienceDirect

Journal of Computational and Applied Mathematics

journal homepage: www.elsevier.com/locate/cam

An adaptive algorithm for the Crank–Nicolson scheme applied to a time-dependent convection–diffusion problem

Marco Picasso *, Virabouth Prachittham

Institut d'Analyse et Calcul Scientifique, École Polytechnique Fédérale de Lausanne, 1015 Lausanne, Switzerland

ARTICLE INFO

Article history:
Received 7 October 2008
Received in revised form 10 August 2009

Keywords:
Adaptive finite elements
A posteriori error estimates
Convection–diffusion
Crank–Nicolson scheme

ABSTRACT

An *a posteriori* upper bound is derived for the nonstationary convection–diffusion problem using the Crank–Nicolson scheme and continuous, piecewise linear stabilized finite elements with large aspect ratio. Following Lozinski et al. (2009) [13], a quadratic time reconstruction is used.

A space and time adaptive algorithm is developed to ensure the control of the relative error in the $l^2(H^1)$ norm. Numerical experiments illustrating the efficiency of this approach are reported; it is shown that the error indicator is of optimal order with respect to both the mesh size and the time step, even in the convection dominated regime and in the presence of boundary layers.

1. Introduction

Deriving robust a posteriori error estimators for stationary convection–diffusion problems with continuous, piecewise linear stabilized finite elements has generated a lot of papers, from both theoretical and experimental point of views, see for instance [1–5] for isotropic meshes and [6–9] for anisotropic meshes. However, fewer papers are available for the nonstationary case, we refer for instance to [10,11].

Concerning parabolic problems and the Crank–Nicolson scheme, it was observed in Section 2.1 of [12] that the standard energy technique yields to a suboptimal a posteriori error estimator. The so-called Crank–Nicolson reconstruction was then introduced in order to restore the appropriate rate of convergence in time. In [13], an alternative piecewise quadratic time reconstruction was proposed, an adaptive space and time algorithm was proposed and numerical results were performed with both error estimators. Moreover, anisotropic finite elements were used.

Our goal is to extend the results presented in [13] to unsteady convection–diffusion problems and to test the quality of our error indicator in the convection dominated regime and in the presence of boundary layers.

The paper is organized as follows. In Section 2 we introduce the model problem and its time and space discretization. Then, we derive in Section 3 an a posteriori upper bound for the error, the involved constant being independent of the time step, mesh size and aspect ratio. In Section 4, a description of the adaptive time and space algorithm is proposed. Finally, in Section 5, we present numerical experiments on several test cases and conclude with the numerical simulation of an electroosmotic flow in a long rectangular channel.

2. The model and its time and space discretization

Let Ω be a polygonal domain with boundary $\partial\Omega$, $T > 0$ the final time, $\epsilon > 0$ the diffusion coefficient, $a : \Omega \times (0, T) \to \mathbb{R}^2$ an incompressible velocity field, $f : \Omega \times (0, T) \to \mathbb{R}$ a source term, $u^0 : \Omega \to \mathbb{R}$ the initial condition. We consider the

* Corresponding author.
E-mail address: marco.picasso@epfl.ch (M. Picasso).

0377-0427/$ – see front matter © 2009 Elsevier B.V. All rights reserved.
doi:10.1016/j.cam.2009.09.004

following problem. Find $u : \Omega \times (0,T) \to \mathbb{R}$ such that

$$\begin{cases} \dfrac{\partial u}{\partial t} - \epsilon \Delta u + a \cdot \nabla u = f & \text{in } \Omega \times (0,T), \\ u = 0 & \text{on } \partial\Omega \times (0,T), \\ u(\cdot,0) = u^0 & \text{in } \Omega. \end{cases} \tag{1}$$

The weak formulation corresponding to (1) is as follows, see for instance [14]. Let W be the functional space defined by

$$W = \{w : \Omega \times (0,T) \to \mathbb{R} \text{ such that } w \in L^2(0,T; H_0^1(\Omega)) \text{ and } \partial w/\partial t \in L^2(0,T; H^{-1}(\Omega))\}.$$

Given $a \in \mathcal{C}^1(\bar{\Omega} \times [0,T])$ such that $\mathrm{div} a = 0, f \in L^2(0,T; H^{-1}(\Omega))$ and $u^0 \in L^2(\Omega)$, we seek for a solution $u \in W$ such that $u(\cdot,0) = u^0$ and

$$\left\langle \frac{\partial u}{\partial t}, v \right\rangle + \epsilon \int_\Omega \nabla u \cdot \nabla v \mathrm{d}x + \int_\Omega (a \cdot \nabla u) v \mathrm{d}x = \langle f, v \rangle \quad \forall v \in H_0^1(\Omega) \text{ and a.e. } t \in (0,T), \tag{2}$$

where $\langle \cdot, \cdot \rangle$ denotes the duality pairing between $H^{-1}(\Omega)$ and $H_0^1(\Omega)$.

It is well know that a standard Galerkin space discretization of (2) leads to spurious oscillations in the convection dominated regime. A remedy is to use a stabilized finite element method, see for instance [15–17] and references therein. In presence of boundary layers, anisotropically refined meshes can be used to improve the precision of the numerical solution with a moderate increase of the number of degrees of freedom.

In this paper, an a posteriori upper bound is derived for a fixed triangulation of Ω. However, in the adaptive algorithm, the triangulation will be changed when necessary. Therefore, the error due to interpolation between meshes will not be considered in this study. The numerical results reported at the end of the paper show that this interpolation error is not important here.

For any $0 < h < 1$, let $\mathcal{T}_h$ be a conforming triangulation of $\overline{\Omega}$ into triangles K with diameter h_K less than h. We define V_h the usual finite element space of continuous, piecewise linear functions on $\mathcal{T}_h$ vanishing on the boundary:

$$V_h = \left\{ v_h \in \mathcal{C}^0(\overline{\Omega});\ v_{h|K} \in P_1;\ \forall K \in \mathcal{T}_h \right\} \cap H_0^1(\Omega).$$

Moreover, in order to approximate the solution of the above problem, we consider the classical Galerkin Least Squares method (GLS) with a modified stabilization parameter due to the use of anisotropic finite elements, see [18] for a theoretical justification in the framework of stationary convection–diffusion. Let $N \geq 1$, we introduce a partition (not necessarily uniform) of the interval $[0,T]$ into subintervals $I_n = [t^{n-1}, t^n]$, $n = 1, \ldots, N$, such that $0 = t^0 < t^1 < \cdots < t^N = T$ and set $\tau_n = t^n - t^{n-1}$. We assume that $f \in \mathcal{C}^0([0,T]; L^2(\Omega))$ and set $f^n(\cdot) = f(\cdot, t^n)$. We also assume that $u^0 \in \mathcal{C}^0(\bar{\Omega})$ and set $u_h^0 = r_h u^0$ where r_h is the Lagrange interpolant corresponding to V_h. Thus, for all $n = 1, \ldots, N$, the Crank–Nicolson scheme consists in seeking $u_h^n \in V_h$ such that for all $v_h \in V_h$ we have

$$\begin{aligned} &\int_\Omega \frac{u_h^n - u_h^{n-1}}{\tau_n} v_h \mathrm{d}x + \frac{\epsilon}{2} \int_\Omega \nabla(u_h^n + u_h^{n-1}) \cdot \nabla v_h \mathrm{d}x + \frac{1}{2} \int_\Omega a \cdot \nabla(u_h^n + u_h^{n-1}) v_h \mathrm{d}x \\ &\quad + \sum_{K \in \mathcal{T}_h} \tau_K \int_K \left(\frac{u_h^n - u_h^{n-1}}{\tau_n} + \frac{1}{2} a \cdot \nabla(u_h^n + u_h^{n-1}) - \frac{1}{2}(f^n + f^{n-1}) \right) (a \cdot \nabla v_h)\, \mathrm{d}x = \frac{1}{2} \int_\Omega (f^n + f^{n-1}) v_h \mathrm{d}x. \end{aligned} \tag{3}$$

The stabilization parameter τ_K is defined by

$$\tau_K = \frac{\lambda_{2,K}}{2|a|_\infty} \xi(Pe_K),$$

where $|a|_\infty = \|a\|_{L^\infty(\Omega \times (0,T))}$ and the function ξ is defined by

$$\xi(Pe_K) = \begin{cases} Pe_K & \text{if } 0 \leq Pe_K \leq 1, \\ 1 & \text{if } 1 \leq Pe_K, \end{cases}$$

with Pe_K, the local Peclet number, defined by

$$Pe_K = \frac{\lambda_{2,K} |a|_\infty}{6\epsilon}.$$

Here $\lambda_{2,K}$ is the local mesh size in the direction of minimum stretching. Its precise definition will be provided in the next section.

3. A posteriori error estimates

3.1. Interpolation estimates for anisotropic finite elements

In order to describe the mesh anisotropy we introduce some definitions and properties taken from [19,20]. Similar results can be found using the framework of [21,22]. For any triangle K of $\mathcal{T}_h$, we consider $T_K : \widehat{K} \to K$, the affine application which maps the reference triangle $\widehat{K}$ into K. Let $M_K \in \mathbb{R}^{2\times 2}$ and $t_K \in \mathbb{R}^2$ be the matrix and the vector defining such a map, we have

$$x = T_K(\hat{x}) = M_K\hat{x} + t_K \quad \forall \hat{x} \in \mathbb{R}^2.$$

Since M_K is invertible, it admits a singular value decomposition

$$M_K = R_K^{\mathrm{T}} \Lambda_K P_K,$$

where R_K and P_K are orthogonal and Λ_K is diagonal with positive entries. In the following we set

$$\Lambda_K = \begin{pmatrix} \lambda_{1,K} & 0 \\ 0 & \lambda_{2,K} \end{pmatrix} \quad \text{and} \quad R_K = \begin{pmatrix} r_{1,K}^{\mathrm{T}} \\ r_{2,K}^{\mathrm{T}} \end{pmatrix} \tag{4}$$

with the choice $\lambda_{1,K} \geq \lambda_{2,K}$. We refer to Section 2 of [23] for examples of such a transformation. The classical minimum angle condition is not required in this context. However, for each vertex, the number of neighboring vertices should be bounded from above, uniformly with respect to the mesh size h. There is another restriction on the mesh (see [8] for a rigorous definition and illustrations) that prevents, loosely speaking, the stretching directions $r_{1,K}$, $r_{2,K}$ from changing too abruptly between the adjacent triangles of the mesh. We suppose in the rest of this paper that the family $\mathcal{T}_h$ meets the above mentioned restrictions. In practice, the BL2D anisotropic mesh generator [24] that we have used meets these restrictions. We now recall some results on interpolation on anisotropic meshes proved in [20,19].

Lemma 1. *Let $I_h : H_0^1(\Omega) \to V_h$ be the Clément interpolation operator [25]. There is a constant C independent of the mesh size and aspect ratio such that, for any $v \in H^1(\Omega)$ and any $K \in \mathcal{T}_h$ we have:*

$$\|v - I_h v\|_{L^2(K)} + \lambda_{2,K}\|\nabla(v - I_h v)\|_{L^2(K)} + \lambda_{2,K}^{1/2}\|v - I_h v\|_{L^2(\partial K)} \leq C\omega_K(v). \tag{5}$$

Here $\omega_K(v)$ is defined by

$$\omega_K^2(v) = \lambda_{1,K}^2 \left(r_{1,K}^{\mathrm{T}} G_K(v) r_{1,K}\right) + \lambda_{2,K}^2 \left(r_{2,K}^{\mathrm{T}} G_K(v) r_{2,K}\right),$$

$\lambda_{i,K}$ and $r_{i,K}$ are given by (4) and $G_K(v)$ is the following 2×2 matrix

$$G_K(v) = \sum_{T\in\Delta_K} \begin{pmatrix} \displaystyle\int_T \left(\frac{\partial v}{\partial x_1}\right)^2 \mathrm{d}x & \displaystyle\int_T \frac{\partial v}{\partial x_1}\frac{\partial v}{\partial x_2}\mathrm{d}x \\ \displaystyle\int_T \frac{\partial v}{\partial x_1}\frac{\partial v}{\partial x_2}\mathrm{d}x & \displaystyle\int_T \left(\frac{\partial v}{\partial x_2}\right)^2 \mathrm{d}x \end{pmatrix},$$

where Δ_K represents the set of triangles of $\mathcal{T}_h$ having a common vertex with K.

3.2. An upper bound for the error based on a three-point reconstruction

For all $n = 1, \ldots, N$, we set

$$\partial_n u_h = \frac{u_h^n - u_h^{n-1}}{\tau_n}, \qquad u_h^{n-1/2} = \frac{1}{2}(u_h^n + u_h^{n-1}),$$

and

$$\partial_n f = \frac{f^n - f^{n-1}}{\tau_n}, \qquad f^{n-1/2} = \frac{1}{2}(f^n + f^{n-1}).$$

Then with these notations, we can rewrite (3) as following

$$\int_\Omega \partial_n u_h v_h \mathrm{d}x + \epsilon \int_\Omega \nabla u_h^{n-1/2} \cdot \nabla v_h \mathrm{d}x + \int_\Omega a \cdot \nabla u_h^{n-1/2} v_h \mathrm{d}x + \sum_{K\in\mathcal{T}_h} \tau_K \int_K \left(\partial_n u_h + a \cdot \nabla u_h^{n-1/2} - f^{n-1/2}\right)(a \cdot \nabla v_h)\,\mathrm{d}x = \int_\Omega f^{n-1/2} v_h \mathrm{d}x. \tag{6}$$

We also introduce the continuous, piecewise linear approximation in time $u_{h\tau}$ defined for all $t \in I_n$ by

$$u_{h\tau}(x,t) = \frac{t-t^{n-1}}{\tau_n}u_h^n + \frac{t^n-t}{\tau_n}u_h^{n-1} = u_h^{n-1/2} + (t-t^{n-1/2})\partial_n u_h, \tag{7}$$

where $t^{n-1/2} = (t^n + t^{n-1})/2$. Thus, for all $v_h \in V_h$, we can rewrite (3) or (6) as

$$\int_\Omega \partial_n u_h v_h \mathrm{d}x + \epsilon \int_\Omega \nabla u_{h\tau}\cdot\nabla v_h \mathrm{d}x + \int_\Omega a\cdot\nabla u_{h\tau} v_h \mathrm{d}x + \sum_{K\in\mathcal{T}_h}\tau_K \int_K \left(\partial_n u_h + a\cdot\nabla u_h^{n-1/2} - f^{n-1/2}\right)(a\cdot\nabla v_h)\,\mathrm{d}x$$
$$= (t-t^{n-1/2})\int_\Omega (\epsilon\nabla\partial_n u_h\cdot\nabla v_h + a\cdot\nabla\partial_n u_h v_h)\,\mathrm{d}x + \int_\Omega f^{n-1/2}v_h \mathrm{d}x. \tag{8}$$

We introduce, $\widetilde{u}_{h\tau}$, the three-point reconstruction defined for all $t \in I_n$, $2 \le n \le N$ by

$$\widetilde{u}_{h\tau}(x,t) = u_{h\tau}(x,t) + \frac{1}{2}(t-t^{n-1})(t-t^n)\partial_n^2 u_h, \tag{9}$$

where

$$\partial_n^2 u_h = \frac{\frac{u_h^n-u_h^{n-1}}{\tau_n} - \frac{u_h^{n-1}-u_h^{n-2}}{\tau_{n-1}}}{(\tau_n+\tau_{n-1})/2}. \tag{10}$$

In order to derive an a posteriori error estimate involving $\widetilde{u}_{h\tau}$, we first need the following result.

Lemma 2. *Set for all $t \in I_n$, $2 \le n \le N$,*

$$\widehat{f} = f^{n-1/2} + (t-t^{n-1/2})\frac{f^n-f^{n-2}}{\tau_n+\tau_{n-1}} \quad \text{and} \quad \widehat{u}_{h\tau} = u_h^{n-1/2} + (t-t^{n-1/2})\frac{u_h^n-u_h^{n-2}}{\tau_n+\tau_{n-1}}.$$

Let $\widetilde{u}_{h\tau}$ be defined by (9) then for all $v_h \in V_h$ and for all $t \in I_n$, $2 \le n \le N$, we have

$$\int_\Omega \frac{\partial\widetilde{u}_{h\tau}}{\partial t}v_h \mathrm{d}x + \epsilon\int_\Omega \nabla u_{h\tau}\cdot\nabla v_h \mathrm{d}x + \int_\Omega a\cdot\nabla u_{h\tau}v_h \mathrm{d}x = \frac{\tau_{n-1}}{2}(t-t^{n-1/2})\int_\Omega \left(\epsilon\nabla\partial_n^2 u_h\cdot\nabla v_h + a\cdot\nabla\partial_n^2 u_h v_h\right)\mathrm{d}x$$
$$+ \int_\Omega \widehat{f}v_h \mathrm{d}x + \sum_{K\in\mathcal{T}_h}\tau_K\int_K\left(\widehat{f} - \frac{\partial\widetilde{u}_{h\tau}}{\partial t} - a\cdot\nabla\widehat{u}_{h\tau}\right)(a\cdot\nabla v_h)\mathrm{d}x.$$

Proof. Let $2 \le n \le N$ and $t \in I_n$. From (9), we have

$$\frac{\partial\widetilde{u}_{h\tau}}{\partial t} = \partial_n u_h + (t-t^{n-1/2})\partial_n^2 u_h. \tag{11}$$

Thus, using (8), we have for all $v_h \in V_h$

$$\int_\Omega \frac{\partial\widetilde{u}_{h\tau}}{\partial t}v_h \mathrm{d}x + \epsilon\int_\Omega \nabla u_{h\tau}\cdot\nabla v_h \mathrm{d}x + \int_\Omega a\cdot\nabla u_{h\tau}v_h \mathrm{d}x + \sum_{K\in\mathcal{T}_h}\tau_K\int_K\left(\partial_n u_h + a\cdot\nabla u_h^{n-1/2} - f^{n-1/2}\right)a\cdot\nabla v_h \mathrm{d}x$$
$$= (t-t^{n-1/2})\int_\Omega \left\{\partial_n^2 u_h v_h + \epsilon\nabla\partial_n u_h\cdot\nabla v_h + a\cdot\nabla\partial_n u_h v_h\right\}\mathrm{d}x + \int_\Omega f^{n-1/2}v_h \mathrm{d}x. \tag{12}$$

We now search for an alternative expression of the first term in the right-hand side of (12). We take the difference between Eq. (3) at time t^n and t^{n-1} to obtain

$$\int_\Omega \partial_n^2 u_h v_h \mathrm{d}x + \epsilon\int_\Omega \nabla\left(\frac{u_h^n-u_h^{n-2}}{\tau_n+\tau_{n-1}}\right)\cdot\nabla v_h \mathrm{d}x + \int_\Omega a\cdot\nabla\left(\frac{u_h^n-u_h^{n-2}}{\tau_n+\tau_{n-1}}\right)v_h \mathrm{d}x$$
$$+ \sum_{K\in\mathcal{T}_h}\tau_K\int_K\left(\partial_n^2 u_h + a\cdot\nabla\left(\frac{u_h^n-u_h^{n-2}}{\tau_n+\tau_{n-1}}\right) - \frac{f^n-f^{n-2}}{\tau_n+\tau_{n-1}}\right)(a\cdot\nabla v_h)\,\mathrm{d}x = \int_\Omega \frac{f^n-f^{n-2}}{\tau_n+\tau_{n-1}}v_h \mathrm{d}x.$$

Thus, as

$$\partial_n u_h - \frac{u_h^n-u_h^{n-2}}{\tau_n+\tau_{n-1}} = \frac{\tau_{n-1}}{2}\partial_n^2 u_h,$$

we have

$$\int_\Omega \left\{\partial_n^2 u_h v_h + \epsilon \nabla \partial_n u_h \cdot \nabla v_h + a \cdot \nabla \partial_n u_h v_h\right\} \mathrm{d}x$$
$$= \frac{\tau_{n-1}}{2} \int_\Omega \left(\epsilon \nabla \partial_n^2 u_h \cdot \nabla v_h + a \cdot \nabla \partial_n^2 u_h v_h\right) \mathrm{d}x + \int_\Omega \left(\frac{f^n - f^{n-2}}{\tau_n + \tau_{n-1}}\right) v_h \mathrm{d}x$$
$$+ \sum_{K \in \mathcal{T}_h} \tau_K \int_K \left(\left(\frac{f^n - f^{n-2}}{\tau_n + \tau_{n-1}}\right) - \partial_n^2 u_h - a \cdot \nabla \left(\frac{u_h^n - u_h^{n-2}}{\tau_n + \tau_{n-1}}\right)\right) (a \cdot \nabla v_h) \, \mathrm{d}x. \tag{13}$$

It suffices now to insert (13) in (12) to obtain the desired result.

The theorem presented hereafter is the main theoretical result of this paper. The proof use the same arguments as in [13]. We reproduce it for the sake of clarity. In what follows we set $e = u - u_{h\tau}$ and $\widetilde{e} = u - \widetilde{u}_{h\tau}$.

Theorem 3. *Let $\widehat{f}$ and $\widehat{u}_{h\tau}$ be defined as in Lemma 2. Assume that the mesh is such that there exists c independent of the time step, mesh size, aspect ratio, ϵ, a, f and u^0 such that*

$$\lambda_{1,K}^2 \left(r_{1,K}^{\mathrm{T}} G_K(\widetilde{e}) r_{1,K}\right) \le c \lambda_{2,K}^2 \left(r_{2,K}^{\mathrm{T}} G_K(\widetilde{e}) r_{2,K}\right) \quad \forall K \in \mathcal{T}_h. \tag{14}$$

Then, there exists C independent of the time step, mesh size, aspect ratio, ϵ, a, f and u^0 such that

$$\int_{t^1}^T \|\nabla e\|_{L^2(\Omega)}^2 \, \mathrm{d}t + \frac{1}{\epsilon} \|e(\cdot, T)\|_{L^2(\Omega)}^2 \le \frac{1}{\epsilon} \left\|e(\cdot, t^1)\right\|_{L^2(\Omega)}^2$$
$$+ C \sum_{n=2}^N \sum_{K \in \mathcal{T}_h} \left\{ \int_{t^{n-1}}^{t^n} \left(\left\| \frac{1}{\epsilon} \left(f - \frac{\partial \widetilde{u}_{h\tau}}{\partial t} - a \cdot \nabla u_{h\tau}\right) + \Delta u_{h\tau} \right\|_{L^2(K)} + \frac{1}{2\lambda_{2,K}^{1/2}} \left\| \left[\frac{\partial u_{h\tau}}{\partial \mathbf{n}}\right] \right\|_{L^2(\partial K)} \right) \omega_K(\widetilde{e}) \mathrm{d}t \right.$$
$$+ \left(\frac{\tau_{n-1}^2 \tau_n^3}{48} + \frac{\tau_n^5}{120}\right) \left(\left\|\nabla \partial_n^2 u_h\right\|_{L^2(K)}^2 + \frac{|a|_\infty^2}{\epsilon^2} \left\|\partial_n^2 u_h\right\|_{L^2(K)}^2 \right) + \int_{t^{n-1}}^{t^n} \left\| \frac{1}{\epsilon} \left(f - \widehat{f}\right) \right\|_{L^2(K)}^2 \mathrm{d}t$$
$$\left. + \frac{|a|_\infty^2 \lambda_{2,K}^4}{\epsilon^2} \int_{t^{n-1}}^{t^n} \left\| \frac{1}{\epsilon} \left(\widehat{f} - \frac{\partial \widetilde{u}_{h\tau}}{\partial t} - a \cdot \nabla \widehat{u}_{h\tau}\right) \right\|_{L^2(K)}^2 \mathrm{d}t \right\}. \tag{15}$$

Here $[\cdot]$ denotes the jump of the bracketed quantity across an internal edge, $[\cdot] = 0$ for an edge on the boundary $\partial\Omega$, and $\mathbf{n}$ is the unit edge normal (in arbitrary direction).

Remark 1. The estimate in Theorem 3 is not a usual a posteriori error estimation since $\widetilde{e} = u - \widetilde{u}_{h\tau}$ (and hence the gradient of u) is still involved in the right-hand side of the estimate. An efficient manner to approximate this quantity was proposed in [8,23] and uses a Zienkiewicz–Zhu post-processing, see Section 3.3 hereafter.

Remark 2. Condition (14) with $c = 1$ will be enforced by our adaptive algorithm, see Section 4 hereafter.

Remark 3. In the case of isotropic meshes $\lambda_{1,K} \simeq \lambda_{2,K} \simeq h_K$, then the above a posteriori error estimate becomes

$$\int_{t^1}^T \|\nabla e\|_{L^2(\Omega)}^2 \, \mathrm{d}t + \frac{1}{\epsilon} \|e(\cdot, T)\|_{L^2(\Omega)}^2 \le \frac{1}{\epsilon} \left\|e(\cdot, t^1)\right\|_{L^2(\Omega)}^2$$
$$+ C \sum_{n=2}^N \sum_{K \in \mathcal{T}_h} \left\{ \int_{t^{n-1}}^{t^n} \left(h_K^2 \left\| \frac{1}{\epsilon} \left(f - \frac{\partial \widetilde{u}_{h\tau}}{\partial t} - a \cdot \nabla u_{h\tau}\right) + \Delta u_{h\tau} \right\|_{L^2(K)}^2 + h_K \left\| \left[\frac{\partial u_{h\tau}}{\partial \mathbf{n}}\right] \right\|_{L^2(\partial K)}^2 \right) \mathrm{d}t \right.$$
$$+ \left(\frac{\tau_{n-1}^2 \tau_n^3}{48} + \frac{\tau_n^5}{120}\right) \left(\left\|\nabla \partial_n^2 u_h\right\|_{L^2(K)}^2 + \frac{|a|_\infty^2}{\epsilon^2} \left\|\partial_n^2 u_h\right\|_{L^2(K)}^2 \right) + \int_{t^{n-1}}^{t^n} \left\| \frac{1}{\epsilon} \left(f - \widehat{f}\right) \right\|_{L^2(K)}^2 \mathrm{d}t$$
$$\left. + \frac{|a|_\infty^2 h_K^4}{\epsilon^2} \int_{t^{n-1}}^{t^n} \left\| \frac{1}{\epsilon} \left(\widehat{f} - \frac{\partial \widetilde{u}_{h\tau}}{\partial t} - a \cdot \nabla \widehat{u}_{h\tau}\right) \right\|_{L^2(K)}^2 \mathrm{d}t \right\}$$

without having to assume (14) but with a constant C depending on the mesh aspect ratio.

Remark 4. We will use the terms in the second line of (15) in order to estimate the error due to space discretization and the terms in the third line of (15) in order to estimate the error due to time discretization. The term in the fourth line of (15) will be disregarded since it is of higher order.

Remark 5. The estimate in Theorem 3 is not robust in the sense of [4,10] since $1/\epsilon$ terms are present in (15). However, the numerical results of Section 5 show that accurate results are obtained even in the convection dominated regime.

Proof. Let $2 \leq n \leq N$ and $t \in I_n$. Using (2), (9) and Lemma 2, we obtain for all $v \in H_0^1(\Omega)$ and all $v_h \in V_h$

$$\begin{aligned}
&\frac{1}{\epsilon}\int_\Omega \frac{\partial \widetilde{e}}{\partial t} v \mathrm{d}x + \int_\Omega \nabla e \cdot \nabla v \mathrm{d}x + \frac{1}{\epsilon}\int_\Omega a \cdot \nabla \widetilde{e} v \mathrm{d}x = \frac{1}{\epsilon}\int_\Omega \left(f - \frac{\partial \widetilde{u}_{h\tau}}{\partial t}\right) v \mathrm{d}x - \int_\Omega \nabla u_{h\tau} \cdot \nabla v \mathrm{d}x - \frac{1}{\epsilon}\int_\Omega a \cdot \nabla \widetilde{u}_{h\tau} v \mathrm{d}x \\
&= \frac{1}{\epsilon}\int_\Omega \left(f - \frac{\partial \widetilde{u}_{h\tau}}{\partial t}\right)(v - v_h)\mathrm{d}x - \int_\Omega \nabla u_{h\tau} \cdot \nabla (v - v_h)\mathrm{d}x - \frac{1}{\epsilon}\int_\Omega a \cdot \nabla u_{h\tau}(v - v_h)\mathrm{d}x \\
&\quad - \frac{1}{2\epsilon}(t - t^{n-1})(t - t^n)\int_\Omega a \cdot \nabla \partial_n^2 u_h v \mathrm{d}x - \frac{\tau_{n-1}}{2}(t - t^{n-1/2})\int_\Omega \left(\nabla \partial_n^2 u_h \cdot \nabla v_h + \frac{1}{\epsilon} a \cdot \nabla \partial_n^2 u_h v_h\right)\mathrm{d}x \\
&\quad + \frac{1}{\epsilon}\int_\Omega (f - \widehat{f}) v_h \mathrm{d}x - \frac{1}{\epsilon}\sum_{K \in \mathcal{T}_h} \tau_K \int_K \left(\widehat{f} - \frac{\partial \widetilde{u}_{h\tau}}{\partial t} - a \cdot \nabla \widehat{u}_{h\tau}\right)(a \cdot \nabla v_h)\mathrm{d}x.
\end{aligned}$$

Note that since a is an incompressible field, we have for all $v \in H_0^1(\Omega)$

$$\int_\Omega a \cdot \nabla v v \mathrm{d}x = 0.$$

Then taking $v = \widetilde{e}$, $v_h = I_h \widetilde{e}$ the Clément interpolant of $\widetilde{e}$ and integrating by parts, we obtain

$$\begin{aligned}
&\frac{1}{2\epsilon}\frac{\mathrm{d}}{\mathrm{d}t}\int_\Omega |\widetilde{e}|^2 \mathrm{d}x + \int_\Omega \nabla e \cdot \nabla \widetilde{e} \mathrm{d}x = \sum_{K \in \mathcal{T}_h}\left\{\int_K \left\{\frac{1}{\epsilon}\left(f - \frac{\partial \widetilde{u}_{h\tau}}{\partial t} - a \cdot \nabla u_{h\tau}\right) + \Delta u_{h\tau}\right\}(\widetilde{e} - I_h \widetilde{e})\mathrm{d}x \right. \\
&\left. + \frac{1}{2}\int_{\partial K}\left[\frac{\partial u_{h\tau}}{\partial \mathbf{n}}\right](\widetilde{e} - I_h \widetilde{e})\mathrm{d}x\right\} + \frac{1}{2\epsilon}(t - t^{n-1})(t - t^n)\int_\Omega a \cdot \nabla \widetilde{e} \partial_n^2 u_h \mathrm{d}x - \frac{\tau_{n-1}}{2}(t - t^{n-1/2}) \\
&\times \int_\Omega \left(\nabla \partial_n^2 u_h \cdot \nabla I_h \widetilde{e} - \frac{1}{\epsilon} a \cdot \nabla I_h \widetilde{e} \partial_n^2 u_h\right)\mathrm{d}x + \int_\Omega \frac{1}{\epsilon}\left(f - \widehat{f}\right) I_h \widetilde{e} \mathrm{d}x \\
&- \sum_{K \in \mathcal{T}_h} \tau_K \int_K \frac{1}{\epsilon}\left(\widehat{f} - \frac{\partial \widetilde{u}_{h\tau}}{\partial t} - a \cdot \nabla \widehat{u}_{h\tau}\right)(a \cdot \nabla I_h \widetilde{e})\mathrm{d}x.
\end{aligned}$$

Using the fact that $ab = \frac{1}{2}a^2 + \frac{1}{2}b^2 - \frac{1}{2}(a-b)^2$, the Cauchy–Schwarz inequality, Lemma 1, the Poincaré inequality, the inequality $ab \leq \frac{1}{2p}a^2 + \frac{p}{2}b^2$, for all $p \in \mathbb{R}^+$ and recall that from (9) we have

$$\|\nabla(e - \widetilde{e})\|_{L^2(K)}^2 = \|\nabla(\widetilde{u}_{h\tau} - u_{h\tau})\|_{L^2(K)}^2 = \frac{1}{4}(t - t^{n-1})^2 (t - t^n)^2 \left\|\nabla \partial_n^2 u_h\right\|_{L^2(K)}^2,$$

then

$$\begin{aligned}
&\frac{1}{2\epsilon}\frac{\mathrm{d}}{\mathrm{d}t}\int_\Omega |\widetilde{e}|^2 \mathrm{d}x + \frac{1}{2}\int_\Omega |\nabla e|^2 \mathrm{d}x + \frac{1}{2}\int_\Omega |\nabla \widetilde{e}|^2 \mathrm{d}x \leq \sum_{K \in \mathcal{T}_h}\left\{C_1\left(\left\|\frac{1}{\epsilon}\left(f - \frac{\partial \widetilde{u}_{h\tau}}{\partial t} - a \cdot \nabla u_{h\tau}\right) + \Delta u_{h\tau}\right\|_{L^2(K)}\right.\right. \\
&\left.\left. + \frac{1}{2\lambda_{2,K}^{1/2}}\left\|\left[\frac{\partial u_{h\tau}}{\partial \mathbf{n}}\right]\right\|_{L^2(\partial K)}\right)\omega_K(\widetilde{e}) + \left\{\frac{p\tau_{n-1}^2}{8}(t - t^{n-1/2})^2 + \frac{1}{8}(t - t^{n-1})^2 (t - t^n)^2\right\}\left\|\nabla \partial_n^2 u_h\right\|_{L^2(K)}^2 \right. \\
&+ \frac{p|a|_\infty^2}{8\epsilon^2}\left\{(t - t^{n-1})^2 (t - t^n)^2 + \tau_{n-1}^2 (t - t^{n-1/2})^2\right\}\left\|\partial_n^2 u_h\right\|_{L^2(K)}^2 + \frac{p}{2}\left\|\frac{1}{\epsilon}\left(f - \widehat{f}\right)\right\|_{L^2(K)}^2 \\
&\left. + \frac{p|a|_\infty^2 \tau_K^2}{2}\left\|\frac{1}{\epsilon}\left(\widehat{f} - \frac{\partial \widetilde{u}_{h\tau}}{\partial t} - a \cdot \nabla \widehat{u}_{h\tau}\right)\right\|_{L^2(K)}^2 + \frac{1}{2p}\|\nabla \widetilde{e}\|_{L^2(K)}^2 + \frac{3 + C_2^2}{2p}\|\nabla I_h \widetilde{e}\|_{L^2(K)}^2\right\},
\end{aligned} \tag{16}$$

where C_1 is the constant of Lemma 1 and C_2 is the constant in the Poincaré inequality. Error equidistribution inequality (14) combined with Lemma 1 implies that

$$\omega_K(\widetilde{e}) \leq C_3 \lambda_{2,K}\|\nabla \widetilde{e}\|_{L^2(K)} \quad \text{and thus} \quad \|\nabla I_h \widetilde{e}\|_{L^2(K)} \leq C_4 \|\nabla \widetilde{e}\|_{L^2(K)}. \tag{17}$$

Finally, we use the second inequality of (17) in (16), the inequality $\tau_K \leq \frac{\lambda_{2,K}^2}{12\epsilon}$, choose $p = 1 + C_4^2(3 + C_2^2)$ and integrate (16) between $t = t^{n-1}$ and $t = t^n$, to obtain

$$\begin{aligned}
&\int_{t^{n-1}}^{t^n} \|\nabla e\|_{L^2(\Omega)}^2 \,\mathrm{d}t + \frac{1}{\epsilon}\left\|\widetilde{e}(\cdot,t^n)\right\|_{L^2(\Omega)}^2 \leq \frac{1}{\epsilon}\left\|\widetilde{e}(\cdot,t^{n-1})\right\|_{L^2(\Omega)}^2 \\
&\quad + C\sum_{K\in\mathcal{T}_h}\left\{\int_{t^{n-1}}^{t^n}\left(\left\|\frac{1}{\epsilon}\left(f - \frac{\partial\widetilde{u}_{h\tau}}{\partial t} - a\cdot\nabla u_{h\tau}\right) + \Delta u_{h\tau}\right\|_{L^2(K)} + \frac{1}{2\lambda_{2,K}^{1/2}}\left\|\left[\!\left[\frac{\partial u_{h\tau}}{\partial \mathbf{n}}\right]\!\right]\right\|_{L^2(\partial K)}\right)\omega_K(\widetilde{e})\mathrm{d}t\right. \\
&\quad + \left(\frac{\tau_{n-1}^2\tau_n^3}{48} + \frac{\tau_n^5}{120}\right)\left(\left\|\nabla\partial_n^2 u_h\right\|_{L^2(K)}^2 + \frac{|a|_\infty^2}{\epsilon^2}\left\|\partial_n^2 u_h\right\|_{L^2(K)}^2\right) \\
&\quad \left. + \int_{t^{n-1}}^{t^n}\left\|\frac{1}{\epsilon}\left(f - \widehat{f}\right)\right\|_{L^2(K)}^2 \mathrm{d}t + \frac{|a|_\infty^2\lambda_{2,K}^4}{\epsilon^2}\int_{t^{n-1}}^{t^n}\left\|\frac{1}{\epsilon}\left(\widehat{f} - \frac{\partial\widetilde{u}_{h\tau}}{\partial t} - a\cdot\nabla\widehat{u}_{h\tau}\right)\right\|_{L^2(K)}^2 \mathrm{d}t\right\},
\end{aligned}$$

where $C = \max(1, 2C_1, p)$. Summing up these inequalities on n and noting that $\widetilde{e}(t^n) = e(t^n)\ \forall n$, leads to the final result.

3.3. An anisotropic error indicator

Since the a posteriori error estimate of Theorem 3 involves the exact solution u we proceed as in [8,23]. Therefore, we introduce the Zienkiewicz–Zhu error estimator [26,27], namely, the difference between $\nabla u_{h\tau}$ and an approximate $L^2(\Omega)$ projection onto V_h:

$$\eta^{ZZ}(u_{h\tau}) = \begin{pmatrix}\eta_1^{ZZ}(u_{h\tau})\\ \eta_2^{ZZ}(u_{h\tau})\end{pmatrix} = \begin{pmatrix}(I - \Pi_h)\left(\dfrac{\partial u_{h\tau}}{\partial x_1}\right)\\ (I - \Pi_h)\left(\dfrac{\partial u_{h\tau}}{\partial x_2}\right)\end{pmatrix},$$

where $\Pi_h(\nabla u_{h\tau}) \in V_h$ is defined by its values at each vertex P as

$$\Pi_h(\nabla u_{h\tau})(P) = \begin{pmatrix}\Pi_h\left(\dfrac{\partial u_{h\tau}}{\partial x_1}\right)(P)\\ \Pi_h\left(\dfrac{\partial u_{h\tau}}{\partial x_2}\right)(P)\end{pmatrix} = \frac{1}{\sum\limits_{\substack{K\in\mathcal{T}_h\\ P\in K}}|K|}\begin{pmatrix}\sum\limits_{\substack{K\in\mathcal{T}_h\\ P\in K}}|K|\left(\dfrac{\partial u_{h\tau}}{\partial x_1}\right)_{|K}\\ \sum\limits_{\substack{K\in\mathcal{T}_h\\ P\in K}}|K|\left(\dfrac{\partial u_{h\tau}}{\partial x_2}\right)_{|K}\end{pmatrix}. \tag{18}$$

Our error indicator is then obtained by replacing $G_K(\widetilde{e})$ in $\omega_K(\widetilde{e})$ by $\breve{G}_K(u_{h\tau})$ defined for any $v_h \in V_h$ by

$$\breve{G}_K(v_h) = \begin{pmatrix}\displaystyle\int_K \left(\eta_1^{ZZ}(v_h)\right)^2 \mathrm{d}x & \displaystyle\int_K \eta_1^{ZZ}(v_h)\eta_2^{ZZ}(v_h)\mathrm{d}x\\ \displaystyle\int_K \eta_1^{ZZ}(v_h)\eta_2^{ZZ}(v_h)\mathrm{d}x & \displaystyle\int_K \left(\eta_2^{ZZ}(v_h)\right)^2 \mathrm{d}x\end{pmatrix}.$$

Approximating in such a way $G_K(\widetilde{e})$ in Theorem 3 and considering Remark 4, we define the anisotropic space error estimator η^A as

$$\eta^A = \left(\sum_{n=1}^{N}\sum_{K\in\mathcal{T}_h}\left(\eta_{K,n}^A(u_{h\tau})\right)^2\right)^{1/2},$$

where the contributions $\eta_{K,n}^A$ are defined on each triangle K of $\mathcal{T}_h$ and each time interval I_n by

$$\begin{aligned}
\left(\eta_{K,n}^A(u_{h\tau})\right)^2 = \int_{t^{n-1}}^{t^n}&\left(\left\|\frac{1}{\epsilon}\left(f - \frac{\partial\widetilde{u}_{h\tau}}{\partial t} - a\cdot\nabla u_{h\tau}\right) + \Delta u_{h\tau}\right\|_{L^2(K)} + \frac{1}{2\lambda_{2,K}^{1/2}}\left\|\left[\!\left[\frac{\partial u_{h\tau}}{\partial \mathbf{n}}\right]\!\right]\right\|_{L^2(\partial K)}\right)\\
&\times\left(\lambda_{1,K}^2\left(r_{1,K}^{\mathrm{T}}\breve{G}_K(u_{h\tau})r_{1,K}\right) + \lambda_{2,K}^2\left(r_{2,K}^{\mathrm{T}}\breve{G}_K(u_{h\tau})r_{2,K}\right)\right)^{1/2}\mathrm{d}t,
\end{aligned} \tag{19}$$

and the time error estimator η^{T} as

$$\eta^{\mathrm{T}} = \left(\sum_{n=2}^{N}\sum_{K\in\mathcal{T}_h}\left(\eta_{K,n}^{\mathrm{T}}(u_{h\tau})\right)^2\right)^{1/2},$$

where the contributions $\eta^{\mathrm{T}}_{K,n}$ are computed on each triangle K of $\mathcal{T}_h$ and each time interval I_n by

$$\left(\eta^{\mathrm{T}}_{K,n}(u_{h\tau})\right)^2 = \left(\frac{\tau_{n-1}^2\tau_n^3}{48} + \frac{\tau_n^5}{120}\right)\left(\left\|\nabla\partial_n^2 u_h\right\|^2_{L^2(K)} + \frac{|a|^2_\infty}{\epsilon^2}\left\|\partial_n^2 u_h\right\|^2_{L^2(K)}\right) + \int_{t^{n-1}}^{t^n}\left\|\frac{1}{\epsilon}\left(f-\widehat{f}\right)\right\|^2_{L^2(K)}\mathrm{d}t,$$

$$\text{for } n \geq 2. \tag{20}$$

Note that in our implementation, all the integrals between t^{n-1} and t^n are approximated by the midpoint rule. Moreover, in order to measure the quality of our estimators, the estimated error is compared to the true error introducing the so-called *effectivity index*. Thus, we define the following effectivity indices in space and time

$$ei^A = \frac{\eta^A}{\left(\int_0^{\mathrm{T}}\int_\Omega |\nabla e|^2\mathrm{d}x\mathrm{d}t\right)^{1/2}} \quad \text{and} \quad ei^{\mathrm{T}} = \frac{\eta^{\mathrm{T}}}{\left(\int_{t^1}^{\mathrm{T}}\int_\Omega |\nabla e|^2\mathrm{d}x\mathrm{d}t\right)^{1/2}}.$$

We will also check the behavior of the Zienkiewicz–Zhu error estimator. We thus introduce the corresponding global estimator and effectivity index

$$\eta^{ZZ} = \left(\sum_{n=1}^{N}\sum_{K\in\mathcal{T}_h}\int_{t^{n-1}}^{t^n}\int_K |\eta^{ZZ}(u_{h\tau})|^2\mathrm{d}x\mathrm{d}t\right)^{1/2} \quad \text{and} \quad ei^{ZZ} = \frac{\eta^{ZZ}}{\left(\int_0^{\mathrm{T}}\int_\Omega |\nabla e|^2\mathrm{d}x\mathrm{d}t\right)^{1/2}}.$$

4. An adaptive algorithm in space and time

The adaptive algorithm described here is quite similar to those presented in [8,13]. The goal is to build successive anisotropic triangulations $\mathcal{T}_h^n$ and choose appropriate time steps τ_n so that the relative error estimated in space and time in the $L^2(0,T;H^1(\Omega))$ norm is close to a preset tolerance TOL, for example

$$0.75\ \mathrm{TOL} \leq \frac{\left((\eta^A)^2+(\eta^{\mathrm{T}})^2\right)^{1/2}}{\left(\int_0^{\mathrm{T}}\int_\Omega |\nabla u_{h\tau}|^2\mathrm{d}x\mathrm{d}t\right)^{1/2}} \leq 1.25\ \mathrm{TOL}. \tag{21}$$

Note that since the time error estimator needs a solution u_h^{n-2}, we do not change the first time step. Thus, sufficient conditions to satisfy the above inequality is that, for all $n \geq 1$, the error indicator in space is such that

$$\begin{aligned}\frac{3}{4}0.75^2\mathrm{TOL}^2\int_{t^{n-1}}^{t^n}\int_\Omega |\nabla u_{h\tau}|^2\mathrm{d}x\mathrm{d}t &\leq \sum_{K\in\mathcal{T}_h}\left(\eta^A_{K,n}(u_{h\tau})\right)^2\\ &\leq \frac{3}{4}1.25^2\mathrm{TOL}^2\int_{t^{n-1}}^{t^n}\int_\Omega |\nabla u_{h\tau}|^2\mathrm{d}x\mathrm{d}t\end{aligned} \tag{22}$$

and, for all $n \geq 2$, the error indicator in time is such that

$$\begin{aligned}\frac{1}{4}0.75^2\mathrm{TOL}^2\int_{t^{n-1}}^{t^n}\int_\Omega |\nabla u_{h\tau}|^2\mathrm{d}x\mathrm{d}t &\leq \sum_{K\in\mathcal{T}_h}\left(\eta^{\mathrm{T}}_{K,n}(u_{h\tau})\right)^2\\ &\leq \frac{1}{4}1.25^2\mathrm{TOL}^2\int_{t^{n-1}}^{t^n}\int_\Omega |\nabla u_{h\tau}|^2\mathrm{d}x\mathrm{d}t.\end{aligned} \tag{23}$$

All the meshes are generated by the BL2D anisotropic mesh software [24] whose also realize the P_1-interpolation between the previous mesh $\mathcal{T}_h^{n-1}$ and the new mesh $\mathcal{T}_h^n$. Thus, BL2D provides us a interpolated solution $r_h^n(u_h^{n-1})$ of u_h^{n-1} on the new mesh, where r_h^n is the Lagrange interpolant operator on $\mathcal{T}_h^n$. We refer to Section 5 of [13] for a complete description of the adaptive procedure where conditions (5.2) and (5.3) of [13] must be replaced by the present conditions (22) and (23). Moreover, we decide not to make the time and space adaptation at the same time. We first carry out the space adaptation before the time adaptation if both conditions (22) and (23) are not satisfied.

Remark 6. Here we do not take into account the interpolation error from mesh $\mathcal{T}_h^{n-1}$ to $\mathcal{T}_h^n$ and conjecture that this error can be neglected provided the total number of remeshings does not depend on the prescribed tolerance TOL. We will observe that this assumption is satisfied in practice.

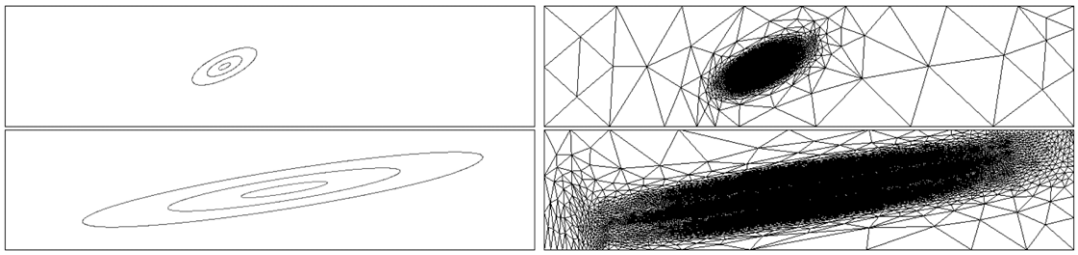

Fig. 1. Example 5.1. Adapted meshes and isovalues obtained with a tolerance TOL = 0.0625. Top: Time $t = 2450$, isovalues 0.1, 0.5, 0.9, with 6421 nodes. Bottom: Final time $T = 9000$, isovalues 0.01, 0.05, 0.1, with 8884 nodes.

5. Numerical experiments

We apply here our adaptive algorithm to several test cases. We monitor at the final time T the absolute error ϵ_{abs} in $L^2(0, T; H^1(\Omega))$ norm, the relative error ϵ_{rel} in the same norm, the number of nodes nb_n, maximum and mean aspect ratio respectively defined by

$$ar = \max_{K\in\mathcal{T}_h} \frac{\lambda_{1,K}}{\lambda_{2,K}} \quad \text{and} \quad \overline{ar} = \frac{\sum_{K\in\mathcal{T}_h} \frac{\lambda_{1,K}}{\lambda_{2,K}}}{\sum_{K\in\mathcal{T}_h} 1}.$$

We also report the number of time steps nb_τ required to reach the final time and the number of remeshings nb_m occurred. We follow [13] Section 6 and do all the computations by replacing ∇u_h^{n-1} by its Zienkiewicz–Zhu recovery, $\Pi_h\left(\nabla u_h^{n-1}\right)$, when $\mathcal{T}_h^{n-1} = \mathcal{T}_h^n$ and ∇u_h^{n-1} by $\Pi_h\left(\nabla r_h^n(u_h^{n-1})\right)$ when $\mathcal{T}_h^{n-1} \neq \mathcal{T}_h^n$ with Π_h defined by (18). In the following section, we study two Examples, 5.1 and 5.2, taken from [28].

Example 5.1. We first consider a problem for which an analytical solution is known. Thus we consider the convection–diffusion of a small source in a plane shear flow. We set $\Omega = (-4000, 26000) \times (-3400, 3400)$, $T = 9000$, $\epsilon = 50$, $f = 0$ and $a = (a_0 + \lambda y, 0)^{\mathrm{T}}$ where $a_0 = 0.5$ and $\lambda = 1\text{e}{-3}$, thus the Peclet number is $|a|_\infty 30000/\epsilon = 2340$. The initial condition u_0 is a point source of mass m at $(x_0, y_0) = (7200, 0)$. Then the solution of (1) is given by

$$u(x, y, t) = \frac{m}{4\pi\epsilon t(1 + \lambda^2 t^2/12)^{1/2}} \exp^{-\chi}, \tag{24}$$

where

$$\chi = \frac{(x - \bar{x} - \lambda y t/2)^2}{4\epsilon t(1 + \lambda^2 t^2/12)} + \frac{y^2}{4\epsilon t} \quad \text{and} \quad \bar{x} = x_0 + a_0 t.$$

To allow the numerical solution of this problem to begin with a finite source size, the computation is started at a time $t = t_0 = 2400$ with

$$m = 4\pi\epsilon t_0(1 + \lambda^2 t_0^2/12)^{1/2}.$$

We present in Fig. 1 the adapted meshes for a tolerance TOL = 0.0625. On Fig. 2 we present a history of the number of nodes and of the time step size against time. We see that the number of nodes is quite constant whereas the time step increases as the solution getting more diffused.

To investigate the efficiency of our adaptive algorithm, we provide in Table 1 (top) numerical experiments with several values of the tolerance TOL. The result show that ei^{ZZ} gets close to one when TOL tends to zero and that the space and time error estimator are equivalent to the true error as their effectivity indices tend to a constant value. We note that the error is divided by two each time the tolerance is and that the optimal second order of convergence with respect to the time step is achieved as the number of time steps is multiplied by $\sqrt{2}$ when TOL is divided by two, see also Fig. 3. We study now the behavior of the same quantities for a smaller diffusion coefficient. We have reported the results in Table 1 (bottom) with a diffusion coefficient $\epsilon = 1$ so that the Peclet number is now 117 000. We can observe that the error is still divided by two each time the tolerance is and that the optimal rate of convergence with respect to the time step is also recovered. The differences concern the Zienkiewicz–Zhu error estimator and the number of nodes and time steps. Indeed, we observe that when the diffusion coefficient gets smaller ei^{ZZ} is not close to one anymore when TOL tends to zero. Regarding the number of nodes and time steps it increase as ϵ decreases which is not surprising according to our space and time indicators. We conclude that our error estimator is sharp, even in the convection dominated regime.

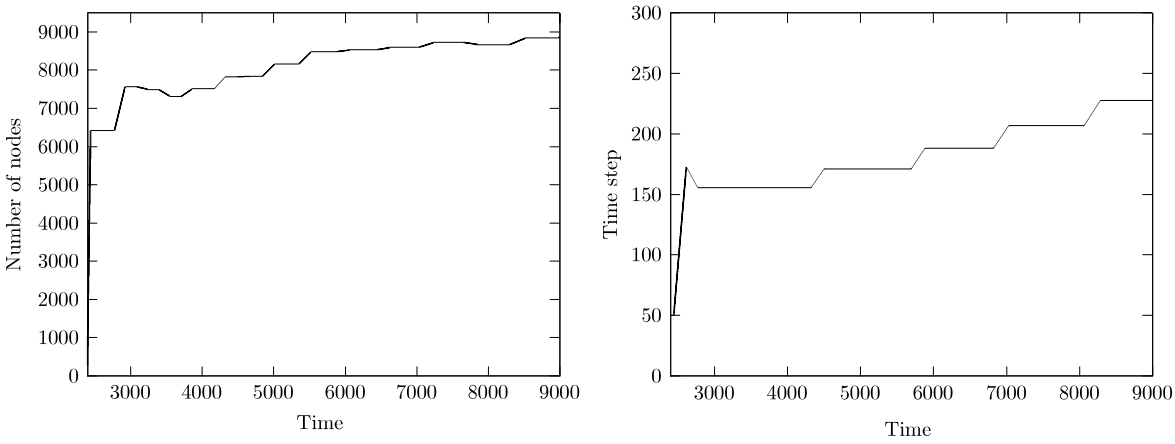

Fig. 2. Example 5.1. Number of nodes (left) and time step (right) with respect to time t with a tolerance TOL $= 0.0625$.

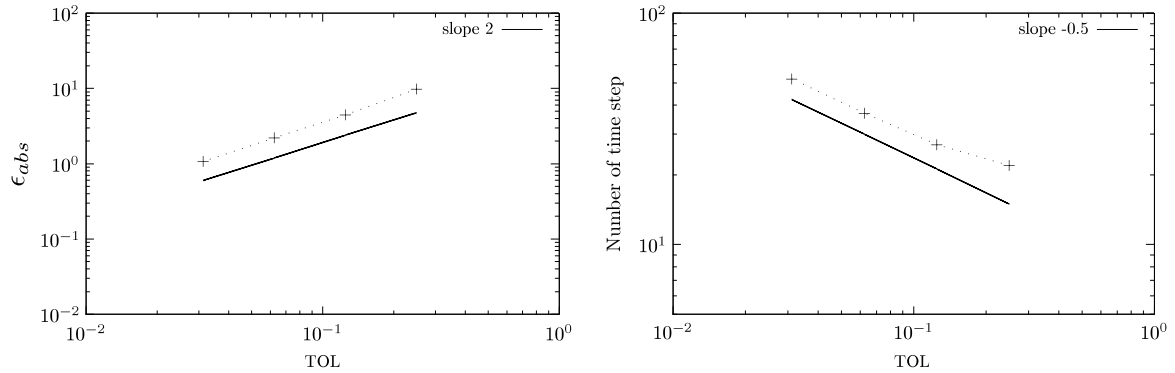

Fig. 3. Example 5.1. True error (left) and total number of time steps (right) at final time $T = 9000$ with respect to the tolerance TOL ($\epsilon = 50$).

Table 1
Example 5.1. True error and effectivity indices of the adapted solution at final time $T = 9000$. Top: $\epsilon = 50$. Bottom: $\epsilon = 1$.

TOL	ϵ_{rel}	ϵ_{abs}	ei^{ZZ}	ei^{A}	ei^{T}	nb_n	nb_τ	nb_m	$\overline{ar}$	ar
0.25	0.110	9.750	0.762	2.131	1.162	1 134	22	20	5.2	27.8
0.125	0.0504	4.475	0.882	2.451	1.072	2 714	27	21	7.3	48.7
0.0625	0.0250	2.218	0.903	2.469	1.154	8 884	37	26	9.5	69.4
0.03125	0.0121	1.073	0.915	2.482	1.137	32 664	52	29	10.1	88.4
0.25	0.116	10.092	0.574	1.93	0.939	1 679	159	44	6.6	48.5
0.125	0.0551	4.856	0.689	2.082	0.978	3 728	206	48	9.7	48.6
0.0625	0.0265	2.344	0.767	2.193	1.082	11 990	281	55	9.9	93.2
0.03125	0.0129	1.144	0.837	2.279	1.163	40 525	400	59	10.6	74.2

Example 5.2. In this example we consider a more anisotropic finite elements test case exhibiting both internal and boundary layers. We set $\Omega = (0, 1)^2$, $f = 0$, $T = 0.6$, $\epsilon = 1\text{e}{-3}$, $a = (2, 1)^{\text{T}}$, $\delta = 7.8125\text{e}{-3}$, thus the Peclet number is $|a|_\infty/\epsilon = 2000$. The initial condition $u^0 = 0$ except on $\partial\Omega$ where u^0 is defined by

$$u^0(x, y) = \begin{cases} 1 & \text{if } x = 0,\ 0 \le y \le 1, \\ 1 & \text{if } 0 \le x \le 1,\ y = 1, \\ (\delta - x)/\delta & \text{if } x \le \delta,\ y = 0, \\ 0 & \text{if } x > \delta,\ y = 0, \\ (y - 1 + \delta)/\delta & \text{if } x = 1,\ y \ge 1 - \delta, \\ 0 & \text{if } x = 1,\ y \le 1 - \delta. \end{cases} \tag{25}$$

Note that we keep the same boundary conditions for the computation of the numerical solution. Thus, this problem exhibits boundary layers along $x = 0$ and $y = 1$ at the initial time. The boundary layer at $x = 0$ propagates into the domain and creates an internal boundary layer which finally reaches the boundary at $x = 1$ and creates a new boundary layer because of the imposed $u = 0$ boundary condition. The boundary layer at $y = 1$ reduces progressively as the solution gets the value of

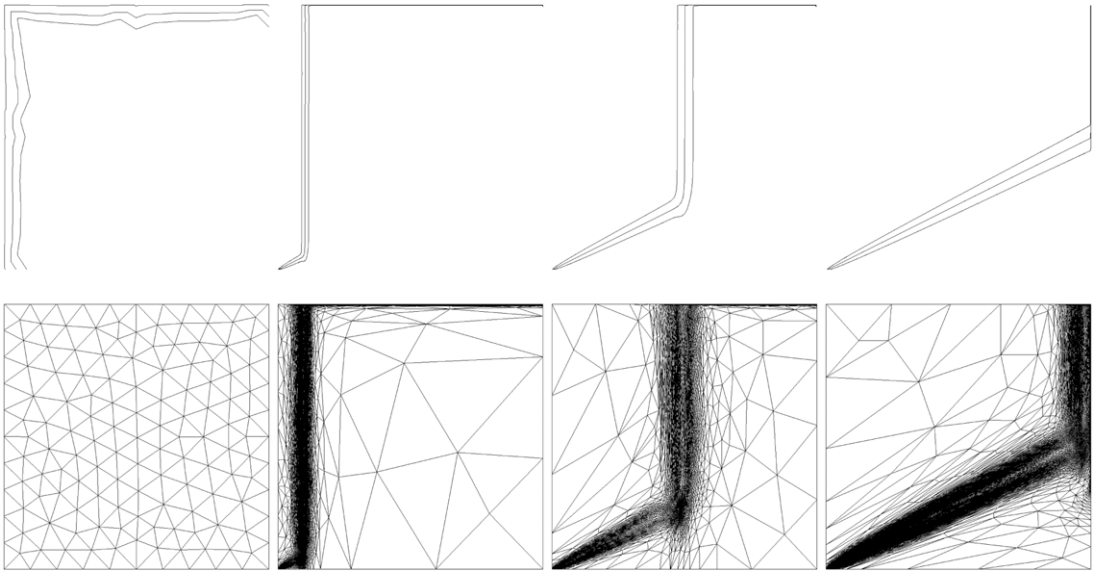

Fig. 4. Example 5.2. Adapted meshes (bottom) and isovalues 0.1, 0.5, 0.9 (top) obtained with a tolerance TOL $= 0.0625$. From left to right: Time $t = 0$, 0.05, 0.25 and 0.6 (151, 9464, 6050 and 38 874 nodes, respectively).

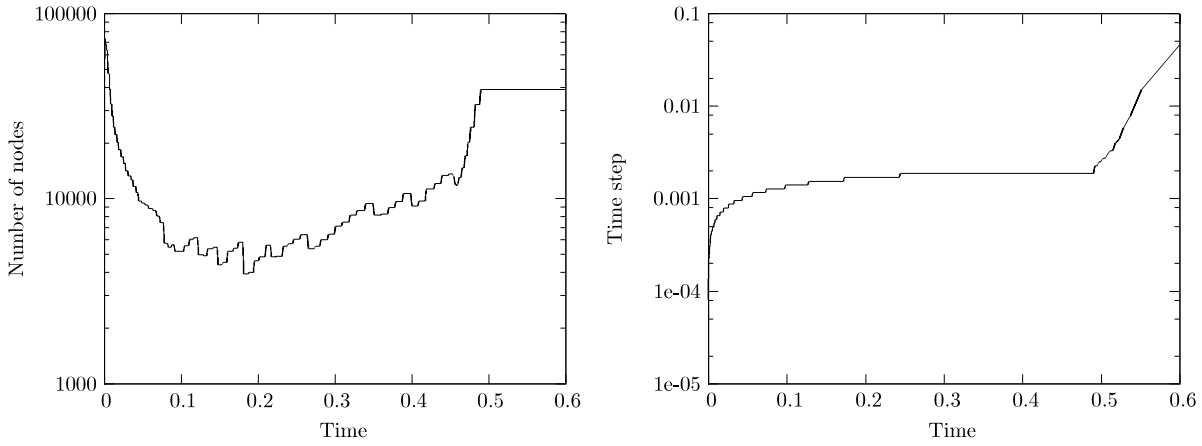

Fig. 5. Example 5.2. Number of nodes (left) and time step (right) with respect to time t with a tolerance TOL $= 0.0625$.

one on the top of the domain. Thus this problem exhibits both internal and boundary layers which make it a very challenging problem. Adapted meshes are presented in Fig. 4 for a tolerance TOL $= 0.0625$. On Fig. 5 we present a history of the number of nodes and of the time step size against time. We see that the number of nodes, initially large due to the discontinuous boundary condition, decreases as the internal layer propagates into the domain and then increases with the development of a new boundary layer at the external boundary until finally becoming constant. For the time step, we see that it was initially very small in order to capture the very large gradient of the solution. Then, progressively it increases as the solution gets more diffused. Moreover, we observe that near the time $t = 0.5$ the solution reaches its stationary point. At this moment, the number of nodes stays constant and the time step increases quickly.

We have reported in Table 2 the total number of time steps required to reach the final time for several values of the tolerance TOL. We observe that the optimal second order of convergence with respect to the time step is recovered as the number of time steps is multiplied by $\sqrt{2}$ when TOL is divided by two, see also Fig. 6. Finally, on Figs. 7 and 8 we present several zooms of the meshes of the numerical simulation reported on Fig. 4. On Fig. 7 we zoom on the left bottom corner and the right top corner of the domain respectively at the time $t = 0.25$ (first and third picture) and the final time $T = 0.6$ (second and fourth picture). On Fig. 8 we present a progressive zoom of the external boundary layer created by the discontinuity of the solution due to the imposed zero value condition on this part of the boundary at the final time $T = 0.6$.

Example 5.3. In this example we study the dynamics of a solute carried by an electroosmotic flow. This kind of motion arises in microfluidic device and is a consequence of the surface charge of a narrow channel. Indeed, at the fluid–solid interfaces, the surface charge attracts the counterions and repels the co-ions and thus creating a thin charged layer known

Table 2
Example 5.2. Number of nodes and time steps of the adapted solution at final time $T = 0.6$.

TOL	nb_n	nb_τ	nb_m	$\overline{ar}$	ar
0.25	3 987	163	93	15.0	190.9
0.125	12 222	247	103	17.9	769.7
0.0625	38 874	353	109	21.6	2553.8
0.03125	140 057	502	130	27.9	9092.1

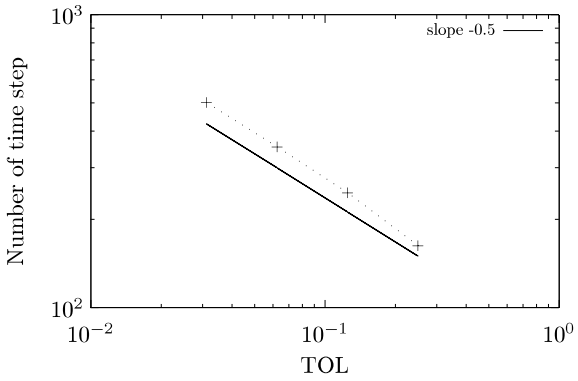

Fig. 6. Example 5.2. Total number of time steps at final time $T = 0.6$ with respect to the tolerance TOL.

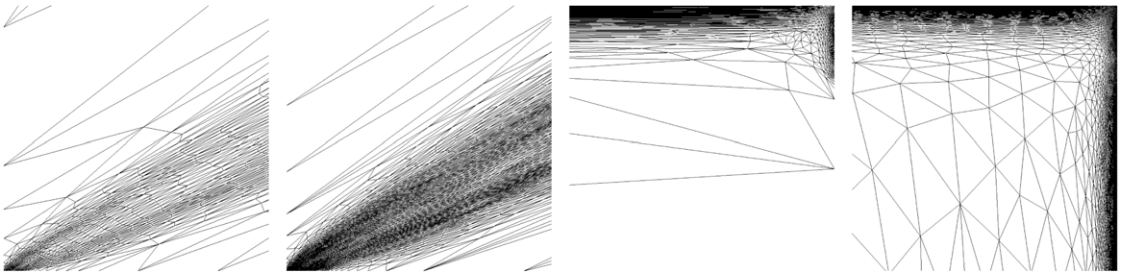

Fig. 7. Example 5.2. Zoom on adapted meshes of the left bottom corner and the right top corner of the domain respectively at the time $t = 0.25$ (first and third pictures) and final time $T = 0.6$ (second and fourth pictures).

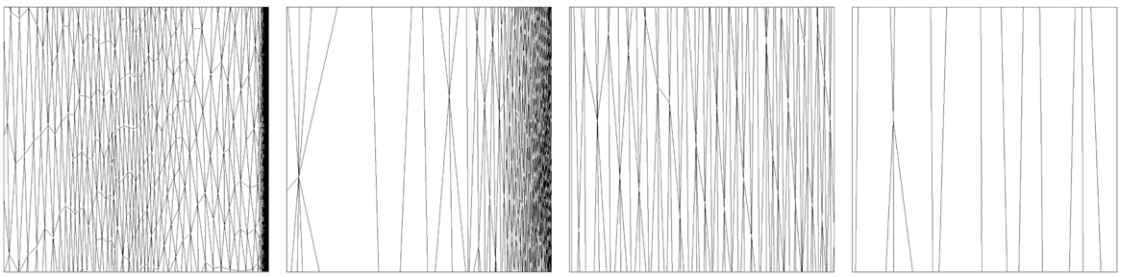

Fig. 8. Example 5.2. From left to right: Zoom of size 1e−1, 1e−2, 1e−3 and 1e−4 of the external boundary layer at $x = 1$ at final time $T = 0.6$.

as the electrical double layer or the Debye layer [29,30]. When an external electric field is applied, the counterions, not attracted by the channel surface, will migrate in the direction of their opposite charge and drag the fluid with them. This is known as electroosmosis. We consider here the numerical simulation of a solute within a rectangular microchannel. All the parameters are given in the international unit system. The solute is initially modelled by a rectangular unit pulse. Thus, we set $\Omega = (0, 6\text{e}{-4}) \times (0, 5\text{e}{-5})$, $\epsilon = 1\text{e}{-10}, f = 0, T = 0.1$. The initial condition u^0 is defined by

$$u^0(x, y) = \begin{cases} 0.5 + 0.5 \tanh\left(\dfrac{x - 1\text{e}{-4}}{1\text{e}{-6}}\right) & \text{if } x < 1.5\text{e}{-4}, \\ 0.5 - 0.5 \tanh\left(\dfrac{x - 2\text{e}{-4}}{1\text{e}{-6}}\right) & \text{if } x > 1.5\text{e}{-4}. \end{cases} \tag{26}$$

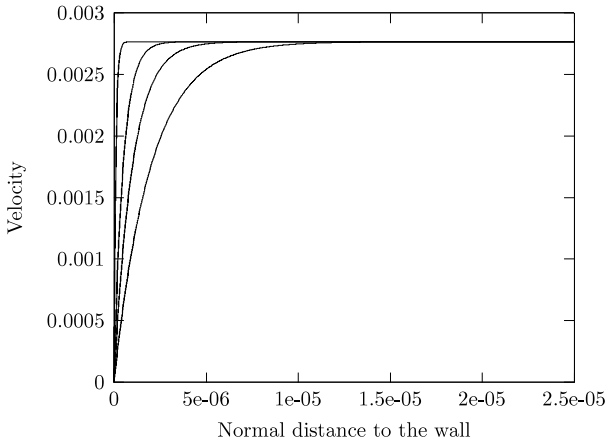

Fig. 9. Example 5.3. Velocity profiles for various values of κ^{-1}. From left to right: $\kappa^{-1} = 1e{-}7, 5e{-}7, 1e{-}6, 2e{-}6$.

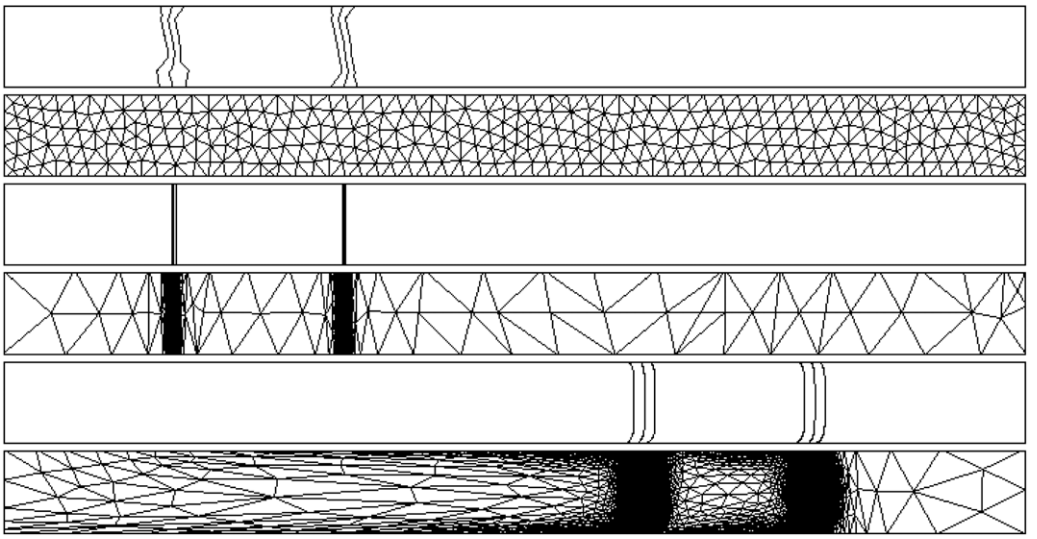

Fig. 10. Example 5.3. Adapted meshes and isovalues 0.1, 0.5 and 0.9 obtained with a tolerance TOL $= 0.0625$. From top to bottom: time $t = 0$, 0.0001, and 0.1 (401, 10 663 and 34 443 nodes, respectively).

Note that we consider here a mixed Dirichlet–Neumann boundary condition problem. Indeed, we impose $u = 0$ along the left and right sides and homogeneous Neumann boundary condition on the top and bottom sides. In the case of a narrow rectangular microchannel with uniformly charged walls and an imposed constant electric field E along the x-direction such as $E = (E_x, 0)^{\mathrm{T}}$, the velocity field is horizontal and given by

$$a(x, y) = \begin{pmatrix} -\dfrac{\varepsilon_0 \zeta E_x}{4\pi\mu}(1 - \exp(-\kappa g(y))) \\ 0 \end{pmatrix}, \tag{27}$$

where $\varepsilon_0 = 6.95e{-}10$ is the electrical permittivity of the solution, $\zeta = -0.1$ is the potential at the wall, $\mu = 1e{-}3$ is the viscosity, $g(y)$ is the normal distance of the wall, $E_x = 5e{+}5$ and κ^{-1} is called the Debye length and it corresponds to the thickness of the Debye layer. Thus the velocity profile is horizontal, equal to zero on the top and bottom sides of the domain, constant in the whole domain except in the Debye layer region very close to the wall. The Peclet number is $|a|_\infty \cdot 5e{-}5/\epsilon = 1385$. On Fig. 9 we plotted the velocity profile against the normal distance to the wall for various values of κ^{-1}.

Note that the Debye thickness (κ^{-1}) is usually of the order 10^{-9}, which will be the value that we will use in our numerical simulations. We can refer to [31,32] for the all set of equations describing the electroosmotic flow in the general case and [29,33] in the case of rectangular microchannels. The numerical simulations are presented in Fig. 10 for a tolerance TOL $= 0.0625$. On Fig. 11 we present the evolution of the number of nodes and of the time step size against time. Here again, the time step size increases with the diffusion of the solution. The number of nodes increases too as the solution gets diffused. In Table 3 we have reported the total number of time steps required to reach the final time for several values of

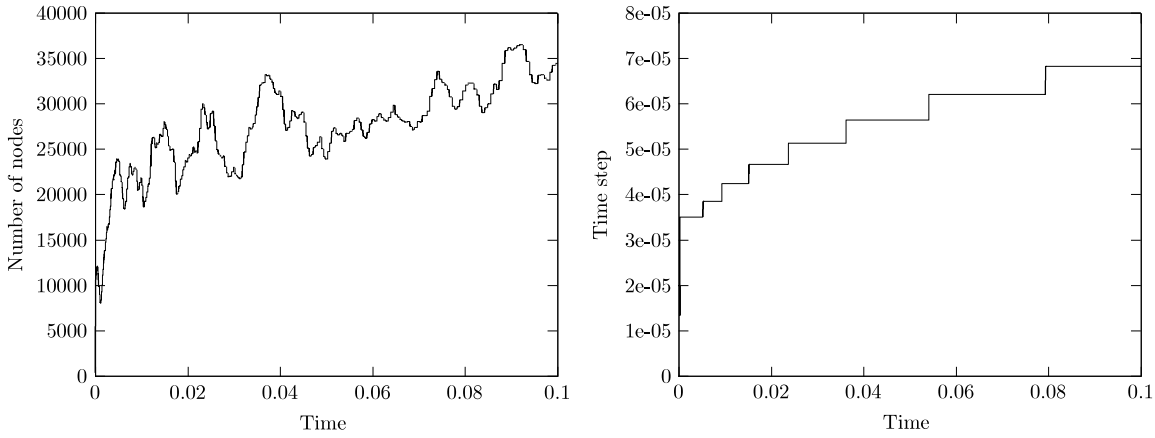

Fig. 11. Example 5.3. Number of nodes (left) and time step (right) with respect to time t with a tolerance TOL $= 0.0625$.

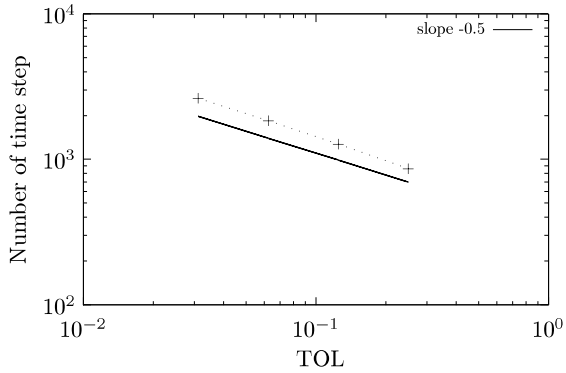

Fig. 12. Example 5.3. Total number of time steps at final time $T = 0.1$ with respect to the tolerance TOL.

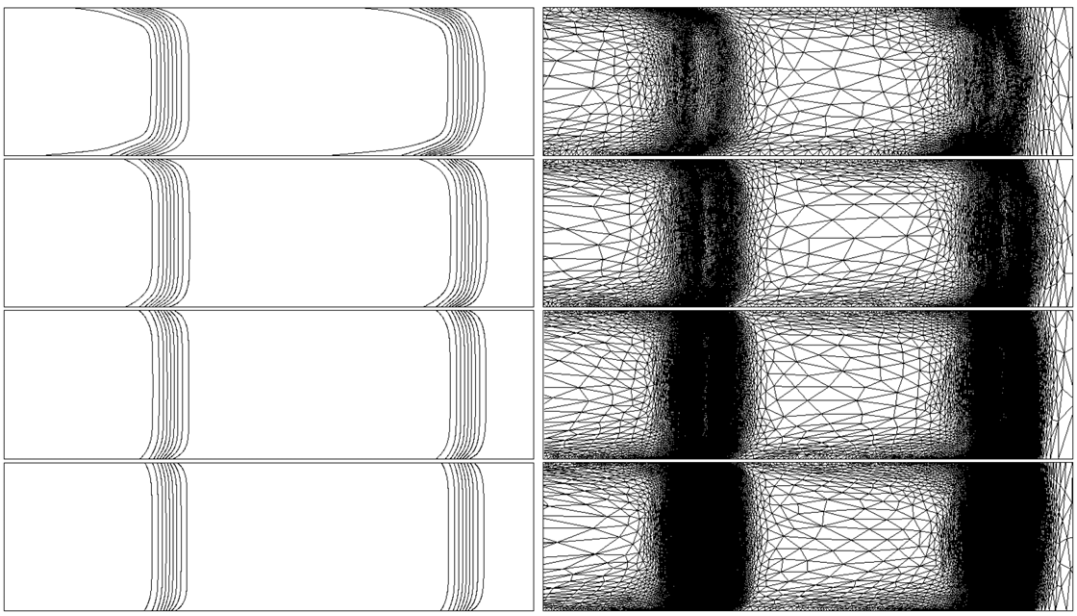

Fig. 13. Example 5.3. Adapted meshes and isovalues 0.1 to 0.9 at final time $T = 0.1$. From top to bottom: tolerance TOL $= 0.25, 0.125, 0.0625, 0.03125$ (10 700, 16 201, 34 443, 60 059 nodes, respectively).

the tolerance TOL. We still observe the optimal second order of convergence with respect to the time step, see also Fig. 12. Finally, on Fig. 13, we zoom on the solute at final time $T = 0.1$ for all the four tolerances of Table 3.

Table 3
Example 5.3. Number of nodes and time steps of the adapted solution at final time $T = 0.1$.

TOL	nb_n	nb_τ	nb_m	$\overline{ar}$	ar
0.25	10700	864	173	4.5	62.1
0.125	16201	1272	240	5.3	49.7
0.0625	34443	1842	290	5.4	63.2
0.03125	60059	2626	316	5.9	78.3

6. Conclusion

An anisotropic error estimator for the time-dependent convection–diffusion problem using the Crank–Nicolson scheme has been derived. The corresponding time and space error estimators have been successfully used in a time and space adaptive algorithm. All the numerical experiments show optimal order with respect to both the mesh size and time step and demonstrate that these indicators provide an efficient tool for the computation of unsteady convection–diffusion problem exhibiting sharp boundary layers.

Acknowledgement

The second author was supported by the Swiss National Science Foundation.

References

[1] V. John, A numerical study of a posteriori error estimators for convection–diffusion equations, Comput. Methods Appl. Mech. Engrg. 190 (5–7) (2000) 757–781.
[2] P. Houston, R. Rannacher, E. Süli, A posteriori error analysis for stabilised finite element approximations of transport problems, Comput. Methods Appl. Mech. Engrg. 190 (11–12) (2000) 1483–1508.
[3] A. Papastavrou, R. Verfürth, A posteriori error estimators for stationary convection–diffusion problems: A computational comparison, Comput. Methods Appl. Mech. Engrg. 189 (2) (2000) 449–462.
[4] R. Verfürth, Robust a posteriori error estimates for stationary convection–diffusion equations, SIAM J. Numer. Anal. 43 (4) (2005b) 1766–1782 (electronic).
[5] G. Sangalli, Robust a-posteriori estimator for advection–diffusion–reaction problems, Math. Comp. 77 (261) (2008) 41–70 (electronic).
[6] L. Formaggia, S. Micheletti, S. Perotto, Anisotropic mesh adaption in computational fluid dynamics: Application to the advection–diffusion–reaction and the Stokes problems, Appl. Numer. Math. 51 (4) (2004) 511–533.
[7] L. Formaggia, S. Perotto, P. Zunino, An anisotropic a-posteriori error estimate for a convection–diffusion problem, in: Second AMIF International Conference (Il Ciocco, 2000), Comput. Vis. Sci. 4 (2) (2001) 99–104.
[8] M. Picasso, An anisotropic error indicator based on Zienkiewicz–Zhu error estimator: Application to elliptic and parabolic problems, SIAM J. Sci. Comput. 24 (4) (2003) 1328–1355 (electronic).
[9] T. Apel, S. Nicaise, A posteriori error estimations of a SUPG method for anisotropic diffusion–convection–reaction problems, C. R. Math. Acad. Sci. Paris 345 (11) (2007) 657–662.
[10] R. Verfürth, Robust a posteriori error estimates for nonstationary convection–diffusion equations, SIAM J. Numer. Anal. 43 (4) (2005a) 1783–1802 (electronic).
[11] S. Micheletti, S. Perotto, Space–time adaption for advection–diffusion–reaction problems on anisotropic meshes. MOX Report 25/2007, 2007.
[12] G. Akrivis, C. Makridakis, R.H. Nochetto, A posteriori error estimates for the Crank–Nicolson method for parabolic equations, Math. Comp. 75 (254) (2006) 511–531.
[13] A. Lozinski, M. Picasso, V. Prachittham, An anisotropic error estimator for the Crank–Nicolson method: Application to a parabolic problem, SIAM J. Sci. Comput. 31 (4) (2009) 2757–2783.
[14] R. Dautray, J.-L. Lions, Evolution Problems II, in: Mathematical Analysis and Numerical Methods for Science and Technology, vol. 6, Springer-Verlag, Berlin, 1993, With the collaboration of Claude Bardos, Michel Cessenat, Alain Kavenoky, Patrick Lascaux, Bertrand Mercier, Olivier Pironneau, Bruno Scheurer and Rémi Sentis, Translated from the French by Alan Craig.
[15] L.P. Franca, S.L. Frey, T.J.R. Hughes, Stabilized finite element methods. I. Application to the advective–diffusive model, Comput. Methods Appl. Mech. Engrg. 95 (2) (1992) 253–276.
[16] R. Codina, Comparison of some finite element methods for solving the diffusion–convection–reaction equation, Comput. Methods Appl. Mech. Engrg. 156 (1–4) (1998) 185–210.
[17] H.-G. Roos, M. Stynes, L. Tobiska, Numerical methods for singularly perturbed differential equations, in: Convection–Diffusion and Flow Problems, in: Springer Series in Computational Mathematics, vol. 24, Springer-Verlag, Berlin, 1996.
[18] S. Micheletti, S. Perotto, M. Picasso, Stabilized finite elements on anisotropic meshes: A priori error estimates for the advection–diffusion and the Stokes problems, SIAM J. Numer. Anal. 41 (3) (2003) 1131–1162 (electronic).
[19] L. Formaggia, S. Perotto, Anisotropic error estimates for elliptic problems, Numer. Math. 94 (1) (2003) 67–92.
[20] L. Formaggia, S. Perotto, New anisotropic a priori error estimates, Numer. Math. 89 (4) (2001) 641–667.
[21] G. Kunert, An a posteriori residual error estimator for the finite element method on anisotropic tetrahedral meshes, Numer. Math. 86 (3) (2000) 471–490.
[22] G. Kunert, R. Verfürth, Edge residuals dominate a posteriori error estimates for linear finite element methods on anisotropic triangular and tetrahedral meshes, Numer. Math. 86 (2) (2000) 283–303.
[23] M. Picasso, Adaptive finite elements with large aspect ratio based on an anisotropic error estimator involving first order derivatives, Comput. Methods Appl. Mech. Engrg. 196 (1–3) (2006) 14–23.
[24] H. Borouchaki, G. Laug, The BL2D mesh generator: Beginner's guide, user's and programmer's manual, Technical Report RT-0194, Institut National de Recherche en Informatique et Automatique (INRIA), Rocquencourt, 78153 Le Chesnay, France, 1996.
[25] P. Clément, Approximation by finite element functions using local regularization, Rev. Fr. Autom. Inform. Rech. Oper. 9 (R-2) (1975) 77–84.
[26] O.C. Zienkiewicz, J.Z. Zhu, A simple error estimator and adaptive procedure for practical engineering analysis, Internat. J. Numer. Methods Engrg. 24 (2) (1987) 337–357.

[27] O.C. Zienkiewicz, J.Z. Zhu, The superconvergent patch recovery and a posteriori error estimates. I. The recovery technique, Internat. J. Numer. Methods Engrg. 33 (7) (1992) 1331–1364.
[28] P. Houston, E. Süli, Adaptive Lagrange–Galerkin methods for unsteady convection–diffusion problems, Math. Comp. 70 (233) (2001) 77–106.
[29] D. Li, Electrokinetics in Microfluidics, Academic Press, New York, USA, 2004.
[30] P.D. Grossman, in: Paul D. Grossman, Joel C. Colburn (Eds.), Capillary Electrophoresis: Theory and Practice, Academic Press, San Diego, CA, USA, 1992.
[31] N. Patankar, H. Hu, Numerical simulation of electroosmotic flow, Anal. Chem. 70 (9) (1998) 1870–1881.
[32] I. Meisel, P. Ehrhard, Electrically-excited (electroosmotic) flows in microchannels for mixing applications, Eur. J. Mech. 25 (4) (2006) 491–504.
[33] S. Ghosal, Electrokinetic flow and dispersion in capillary electrophoresis, Annu. Rev. Fluid Mech. 38 (1) (2006) 309–338.